Supplementary materials for the article: Acoustic spectra of a gas-filled rotating spheroid

S. Su, D. Cébron, H-C. Nataf, P. Cardin, J. Vidal, M. Solazzo, Y. Do

October 2019

Supplementary materials

Contents

1 Governing (aero-acoustic) linearized equations **2**

2 Ellipticity perturbation theory **3**
2.1 Shape functions of an oblate spheroid 3
2.2 First-order ellipticity correction 3
2.3 Second-order ellipticity correction 5
2.4 MATLAB package 5

3 Elastic effects of the container **7**

4 Numerical values for ZoRo's acoustic modes **8**

5 Finite-element calculations with COMSOL Multiphysics **9**
5.1 Built-in COMSOL (version 5.4) capabilities and limitations 9
5.2 How to calculate COMSOL axisymmetric aero-acoustic modes with $m \neq 0$? 9
5.3 Boundary conditions and details on the numerics 10
5.4 Elastic container, boundary coupling and sound radiation in the surrounding outer fluid 11

6 Mode identification on experimental spectrum (complement to Fig. 2 of the main text) **12**

7 Comparison of acoustic spectra from experiment, theory and finite-element calculations (complement to Fig. 6 of the main text) **13**

8 Examples of spectral fitting (complement to Fig. 8 of the main text) **14**

9 Ledoux coefficients for a collection of symmetric and anti-symmetric modes (complement to Fig. 9 of the main text) **16**

1 Governing (aero-acoustic) linearized equations

Considering a homogeneous basic (background) state of density ρ_0, pressure p_0, velocity $\boldsymbol{u}_0$, and temperature T_0, we study small perturbations $[\rho, p, \boldsymbol{u}, T]$ of these respective quantities. In a frame rotating at $\boldsymbol{\Omega}$, we can thus linearize the governing flow equations for a Newtonian fluid, leading to the so-called aero-acoustic linearized equations (Blackstock, 2001)

$$\partial_t \rho + \nabla \cdot (\rho_0 \boldsymbol{u} + \rho \boldsymbol{u_0}) = M \tag{1}$$

$$\begin{aligned} \rho_0 \left[\partial_t \boldsymbol{u} \right. &+ \left. \boldsymbol{u_0} \cdot \nabla \boldsymbol{u} + \boldsymbol{u} \cdot \nabla \boldsymbol{u_0} + 2\boldsymbol{\Omega} \times \boldsymbol{u}\right] \\ &+ \rho \left[(\boldsymbol{u_0} \cdot \nabla \boldsymbol{u_0}) + 2\boldsymbol{\Omega} \times \boldsymbol{u_0} + \boldsymbol{\Omega} \times (\boldsymbol{\Omega} \times \boldsymbol{r})\right] \\ &= \nabla \cdot \Big(-p\mathbf{I} + \mu[\nabla \boldsymbol{u} + (\nabla \boldsymbol{u})^\top] + \mu_2 (\nabla \cdot \boldsymbol{u})\mathbf{I}\Big) + \rho \boldsymbol{g} + \boldsymbol{F} \end{aligned} \tag{2}$$

$$\begin{aligned} \rho_0 C_p \left[\partial_t T \right. &+ \left. \boldsymbol{u_0} \cdot \nabla T + \boldsymbol{u} \cdot \nabla T_0\right] + \rho C_p \, \boldsymbol{u_0} \cdot \nabla T_0 \\ &- \alpha T_0 \left[\partial_t p + \boldsymbol{u_0} \cdot \nabla p + \boldsymbol{u} \cdot \nabla p_0\right] - \alpha T \, \boldsymbol{u_0} \cdot \nabla p_0 \\ &= \nabla \cdot (\lambda \nabla T) + Q, \end{aligned} \tag{3}$$

with the position vector $\boldsymbol{r}$, and with the usual linearized equation of state $\rho = \rho_0(\beta_T p - \alpha T)$ for a gas, with the (isobaric) coefficient of thermal expansion α, the identity $\mathbf{I}$, the specific heat at constant pressure C_p, the thermal conductivity λ, and where M, $\boldsymbol{F}$, Q are possible source terms ($\boldsymbol{g}$ being the gravity). In these equations, μ is the dynamic (shear) viscosity and the second coefficient of viscosity μ_2 is related to the bulk viscosity μ_B by $\mu_2 = \mu_B - 2\mu/3$. In these equations also appears the isothermal compressibility $\beta_T = \gamma \beta_s$, where γ is the specific-heat ratio and β_s is the isentropic compressibility (also called fluid compressibility). The speed of sound is then $c = (\rho_0 \beta_s)^{-1/2} = [\gamma/(\rho_0 \beta_T)]^{1/2}$, and the heat capacity at constant volume C_v is $C_v = C_p/\gamma$. For the air in standard condition, we have typically $\mu_B = 0.6\mu$ for air (p. 315 of Blackstock, 2001), $\gamma = 1.4$, and $\beta_T = 1/p_0$ (for an ideal gas). Note also that we assume diffusion coefficients to be uniform and constant in all our study.

Noting the gravity acceleration $\boldsymbol{g}$, one can define a local gravity force as

$$(\rho_0 + \rho)\boldsymbol{g}_l = (\rho_0 + \rho)[\boldsymbol{g} - \boldsymbol{\Omega} \times (\boldsymbol{\Omega} \times \boldsymbol{r})]. \tag{4}$$

Since the force term $\rho_0 \boldsymbol{g}_l$ is directly balanced by the pressure term ∇p_0 in the diffusionless version of equation (2), we choose to neglect the effects of $\boldsymbol{g}_l$ on the background state and on the perturbation dynamics. These usual assumptions allow (i) to consider a homogeneous background state, and (ii) to neglect the gravity as well as the centrifugal acceleration in equation (2). The hypothesis (i) is valid if the scale height $H_s = 1/(\beta_T \rho_0 g_l)$ is large compared to the size $r_{eq} = 0.2$ m of the experiment (Tritton, 2012). This is the case since $H_s \approx 12$ m for a rotation rate of $f_\Omega = 30$ Hz, using $\beta_T = 1/p_0$ and the ambient atmospheric pressure $p_0 = 10^5$ Pa. The assumption (ii) is valid if, in equation (2), the centrifugal term ρg_l is small compared to the Coriolis term $2\rho_0 \Omega u$, where $\omega \rho \approx \rho_0 u / r_{eq}$ according to equation (1). This is valid when $\omega/\Omega \gg 1$ and $g/(\Omega \omega r_{eq}) \ll 1$, which is true in our case since $f_\Omega \leq 30$ Hz and the fundamental eigenfrequency is larger than 500 Hz, leading to $g/(\Omega \omega r_{eq}) \leq 10^{-4}$.

In our work, we also neglect in equation (3) the viscous heating, i.e. the viscous dissipation function $\phi = (\nabla \boldsymbol{u}) : \boldsymbol{\tau}$, where $\boldsymbol{\tau} = \mu[\nabla \boldsymbol{u} + (\nabla \boldsymbol{u})^\top] + \mu_2 (\nabla \cdot \boldsymbol{u})\mathbf{I}$ is the dissipative part of the stress tensor $\boldsymbol{\sigma} = -p\mathbf{I} + \boldsymbol{\tau}$. One can wonder if this is valid in our case. The viscous heating power P_μ can be estimated by $P_\mu \approx \phi r_{eq}^3 \approx \rho_0 \omega u^2 r_{eq}^3$, where $u \approx r_{eq} \omega \rho / \rho_0$ according to equation (1). In all our experiments, our pressure measurements remain below $p_{max} = 0.1$ Pa, obtained around $f_\Omega = 1$ kHz, which gives $\rho/\rho_0 \leq 10^{-6}$ and then $P_\mu = \rho_0 r_{eq}^5 \omega^3 (\rho/\rho_0)^2 \leq 0.1$ mW. Compared to the speakers input power of 3 W, this confirms that P_μ is negligible in all our experiments.

2 Ellipticity perturbation theory

We follow the approach detailed in Mehl (2007)'s brilliant paper that applies the formalism of Morse and Feshbach (1953) to infer the frequency shift experienced by spherical acoustic modes in a slightly deformed sphere. Mehl extended the perturbation theory to the second order, focusing on $l = 0$ and $l = 1$ modes.

The shape of the aspherical cavity is given by the evolution of the radius r_s of its boundary with θ and φ as:

$$r_s = r_{eq}[1 - \epsilon\mathcal{F}(\theta, \varphi)], \tag{5}$$

where $\mathcal{F}$ is a smooth positive function of order 1 and ϵ is a small positive parameter, which serves as the expansion parameter. The shape function $\mathcal{F}$ itself is expanded in ϵ as:

$$\mathcal{F} = \mathcal{F}_0 + \epsilon\mathcal{F}_1 + O(\epsilon^2). \tag{6}$$

We have adapted Mehl's method to obtain the first-order and second-order frequency perturbations for modes of any l in an axisymmetric spheroid.

2.1 Shape functions of an oblate spheroid

Given the equatorial radius r_{eq} and the polar radius r_{pol} of an oblate axisymmetric spheroid (such as ZoRo), the cross-sections are elliptical with:

$$\left(\frac{x}{r_{eq}}\right)^2 + \left(\frac{y}{r_{pol}}\right)^2 = 1, \tag{7}$$

which can be written as

$$r_s = \frac{r_{pol}}{\sqrt{1 + (2\epsilon + \epsilon^2)\cos^2\theta}}, \tag{8}$$

correcting a typo for equation (53) of Mehl (2007). with ϵ here defined as $\epsilon = r_{eq}/r_{pol} - 1 = e/(1-e) = e\, r_{eq}/r_{pol}$, using the ellipticity e defined in the main text.

Combining with equations (5) and (8), we get

$$\mathcal{F} = \cos^2\theta + \epsilon\left(\frac{1}{2}\cos^2\theta - \frac{3}{2}\cos^4\theta\right) + O(\epsilon^2), \tag{9}$$

i.e. equation (54) of Mehl (2007).

The perturbation method of Mehl (2007) uses an expansion of the shape functions into spherical harmonics. We thus expand the functions $\mathcal{F}_0$, $\mathcal{F}_1$ and $\mathcal{F}_0^2$ into fully normalised spherical harmonics as

$$\begin{aligned}
\mathcal{F}_0 &= \frac{2}{3}\sqrt{\pi}\,\mathcal{Y}_0^0 + \frac{4}{3}\sqrt{\frac{\pi}{5}}\,\mathcal{Y}_2^0, \\
\mathcal{F}_1 &= -\frac{4}{15}\sqrt{\pi}\,\mathcal{Y}_0^0 - \frac{22}{21}\sqrt{\frac{\pi}{5}}\,\mathcal{Y}_2^0 - \frac{8}{35}\sqrt{\pi}\,\mathcal{Y}_4^0, \\
\mathcal{F}_0^2 &= \frac{2}{5}\sqrt{\pi}\,\mathcal{Y}_0^0 + \frac{8}{7}\sqrt{\frac{\pi}{5}}\,\mathcal{Y}_2^0 + \frac{16}{105}\sqrt{\pi}\,\mathcal{Y}_4^0.
\end{aligned} \tag{10}$$

The averages over solid angle, noted $\langle\cdot\rangle$, are given by equation (55) of Mehl (2007), after correcting his value for $\langle\mathcal{F}_1\rangle$, yielding

$$\langle\mathcal{F}_0\rangle = \frac{1}{3}, \quad \langle\mathcal{F}_1\rangle = -\frac{2}{15}, \quad \langle\mathcal{F}_0^2\rangle = \frac{1}{5}. \tag{11}$$

2.2 First-order ellipticity correction

At first-order in ϵ, the radial eigenvalue $k_{nlm}^{(1)}$ of mode ${}_n\mathcal{S}_l^m$ in an aspherical cavity defined by (8) and (6) is given by:

$$\frac{[k_{nlm}^{(1)}]^2 - k_{nl}^2}{k_{nl}^2} = \epsilon\, SC_{nlm}^{(1)}, \tag{12}$$

where the first-order self-coupling term is given by

$$SC^{(1)}_{nlm} = 2\frac{\int \left[z^2_{nl}\,|\mathcal{Y}^m_l|^2\,\mathcal{F}_0 - |r\nabla\mathcal{Y}^m_l|^2\,\mathcal{F}_0\right]\mathrm{d}\Omega}{z^2_{nl} - l(l+1)}, \tag{13}$$

where $\int \mathrm{d}\Omega$ represents the integral over solid angle, and $z_{nl} = k_{nl}a$ is the n^{th} root of j'_l the first derivative of j_l the spherical Bessel function of the first kind, and a the radius of the reference sphere. A term equal to $-2\langle\mathcal{F}_0\rangle$ must be added to the right hand-side of equation (13) if one uses a reference sphere with the same volume as the aspherical cavity, i.e. with $a = \sqrt[3]{r_{pol}r^2_{eq}}$ (Mehl, 2007).

The shape function $\mathcal{F}_0(\theta,\varphi)$ can be expanded in spherical harmonics as

$$\mathcal{F}_0 = \sum_{l_0,\,m_0} F^{m_0}_{l_0}\mathcal{Y}^{m_0}_{l_0}, \tag{14}$$

transforming the integrals over solid angle of equation (13) into a sum of Gaunt integrals. It is convenient to introduce the following functions:

$$A^{mm'}_{ll'}(\mathcal{F}_0) = 2\sum_{l_0,\,m_0} F^{m_0}_{l_0}\int \mathcal{Y}^{m_0}_{l_0}\left[\mathcal{Y}^{m'}_{l'}\right]^*\mathcal{Y}^m_l\,\mathrm{d}\Omega, \tag{15}$$

$$B^{mm'}_{ll'}(\mathcal{F}_0) = -2\sum_{l_0,\,m_0} F^{m_0}_{l_0}\int \mathcal{Y}^{m_0}_{l_0}\left[r\nabla\mathcal{Y}^{m'}_{l'}\right]^*\cdot r\nabla\mathcal{Y}^m_l\,\mathrm{d}\Omega. \tag{16}$$

where * stands for the complex conjugate. Then, we rewrite equation (13) as

$$SC^{(1)}_{nlm} = \frac{z^2_{nl}A^{mm}_{ll}(\mathcal{F}_0) + B^{mm}_{ll}(\mathcal{F}_0)}{z^2_{nl} - l(l+1)}. \tag{17}$$

While Mehl (2007) used symbolic algebra to combine the contributions of the non-zero coefficients in equation (13), we choose to express the solid angle integrals of equations (15) and (16) as Gaunt-type integrals, which are related to Wigner 3j symbols by:

$$\int \mathcal{Y}^{m_1}_{l_1}\left(\mathcal{Y}^{m_2}_{l_2}\right)^*\mathcal{Y}^{m_3}_{l_3}\,\mathrm{d}\Omega = (-1)^{m_1}\sqrt{\frac{(2l_1+1)(2l_2+1)(2l_3+1)}{4\pi}}\begin{pmatrix} l_1 & l_2 & l_3\\ 0 & 0 & 0\end{pmatrix}\begin{pmatrix} l_1 & l_2 & l_3\\ m_1 & -m_2 & m_3\end{pmatrix} \tag{18}$$

and

$$\int \left(r\nabla\mathcal{Y}^{m_1}_{l_1}\right)\cdot\left(r\nabla\mathcal{Y}^{m_2}_{l_2}\right)^*\mathcal{Y}^{m_3}_{l_3}\,\mathrm{d}\Omega = -\frac{-l_1(l_1+1) - l_2(l_2+1) + l_3(l_3+1)}{2}\int \mathcal{Y}^{m_1}_{l_1}\left(\mathcal{Y}^{m_2}_{l_2}\right)^*\mathcal{Y}^{m_3}_{l_3}\mathrm{d}\Omega \tag{19}$$

with the fully normalised spherical harmonics defined in Dahlen and Tromp (1998), p. 917.

For an oblate spheroid, equations (10) show that the first-order shape function $\mathcal{F}_0$ only contains $\mathcal{Y}^0_0$ and $\mathcal{Y}^0_2$ contributions. Dahlen (1968) showed that the first-order frequency shift of an m-singlet is then proportional to m^2, yielding

$$\frac{\delta_{geom}}{f_{nl}} = \left(\frac{1}{2} - \frac{3m^2}{2l(l+1)}\right)\epsilon\left[SC^{(1)}_{nl0} - 2\langle\mathcal{F}_0\rangle\right], \tag{20}$$

so that the $SC^{(1)}_{nlm}$ term only needs being calculated for $m = 0$. Dahlen (1968) also provides integral expressions to calculate $\gamma_{nl} \equiv -\frac{3}{2l(l+1)}\left(SC^{(1)}_{nl0} - 2\langle\mathcal{F}_0\rangle\right)$ in the more general situation of Earth's normal modes. However, Dahlen and Tromp (1998) recall that they contain errors, which have been corrected in Dahlen (1976). We checked that we obtain the same values, using the expressions of either Mehl (2007) or Dahlen (1976), taking into account their different definitions of ellipticity.

However, as shown in the main text, first-order corrections are not sufficient to provide a fair estimate for the frequencies of the acoustic singlets, for the flattening of our ZoRo experiment.

2.3 Second-order ellipticity correction

The formalism presented by Morse and Feshbach (1953) extends to second-order. Mehl (2007) developed the mathematical tools to calculate these terms for spheroids. He provided a very elaborate assessment of all required terms, and we closely follow his approach again. The aspherical eigenvalues correct at second-order in ϵ are given by

$$\frac{[k^{(2)}_{nlm}]^2 - k^2_{nl}}{k^2_{nl}} = \epsilon SC^{(1)}_{nlm} + \epsilon^2 \left(SC^{(2)}_{nlm} + CC^{(2)}_{nlm} \right). \tag{21}$$

In contrast to first-order, second-order corrections for a given ${}_n\mathcal{S}^m_l$ mode involve coupling with several ${}_{n'}\mathcal{S}^{m'}_{l'}$ modes. Thus, second-order corrections stem from both the second-order self-coupling term $SC^{(2)}_{nlm}$ and the $CC^{(2)}_{nlm}$ cross-coupling term.

Expanding $\mathcal{F}_1$ and $\mathcal{F}_0^2$ in spherical harmonics as in equation (14), the self-coupling second-order contribution can be written, using functions defined in equations (15)–(16), as

$$SC^{(2)}_{nlm} = \frac{z^2_{nl} A^{mm}_{ll}(\mathcal{F}_1 - \mathcal{F}_0^2) + B^{mm}_{ll}(\mathcal{F}_1)}{z^2_{nl} - l(l+1)} + \frac{z^2_{nl} A^{mm}_{ll}(\mathcal{F}_0) + B^{mm}_{ll}(\mathcal{F}_0)}{z^2_{nl} - l(l+1)} \cdot \frac{z^2_{nl} A^{mm}_{ll}(\mathcal{F}_0)}{z^2_{nl} - l(l+1)}. \tag{22}$$

A term equal to $-\langle \mathcal{F}_0 \rangle^2 + 2\langle \mathcal{F}_0^2 \rangle - 2\langle \mathcal{F}_1 \rangle - 2\langle \mathcal{F}_0 \rangle SC^{(1)}_{nlm}$ must be added to $SC^{(2)}_{nlm}$ if one uses a reference sphere with the same volume as the aspherical cavity. The cross-coupling contribution is

$$CC^{(2)}_{nlm} = \frac{\sum\limits_{l'm'} |z^2_{nl} A^{mm'}_{ll'}(\mathcal{F}_0) + B^{mm'}_{ll'}(\mathcal{F}_0)|^2 S_{nll'}}{z^2_{nl} - l(l+1)} + \frac{|z^2_{nl} A^{m0}_{l0}(\mathcal{F}_0) + B^{m0}_{l0}(\mathcal{F}_0)|^2}{2 z^2_{nl} \left[z^2_{nl} - l(l+1) \right]}, \tag{23}$$

where the $S_{nll'}$ sums up the contribution of all l'-modes with radial mode number $n' \neq n$.

The $S_{lnl'}$ sums are the only elements that are linked to the radial functions, and they are evaluated explicitly by Mehl (2007). For completeness, we recall their expressions in the following. For $l' \neq 0$, we have

$$\begin{aligned} S_{lnl'} &= -\frac{j_{l'}(z_{nl})}{2\, z_{nl}\, j'_{l'}(z_{nl})} \qquad \text{for } l' \neq l, \\ S_{lnl} &= \frac{z^2_{nl} - 3l(l+1)}{4 \left[z^2_{nl} - l(l+1) \right]^2} \quad \text{for } l' = l, \end{aligned} \tag{24}$$

For $l' = 0$, we have

$$\begin{aligned} S_{ln0} &= -\frac{1}{2\, z^2_{nl}} - \frac{j_0(z_{nl})}{2\, z_{nl}\, j'_0(z_{nl})} \quad \text{for } l \neq 0, \\ S_{0n0} &= -\frac{1}{4\, z^2_{n0}} \qquad\qquad\qquad\quad \text{for } l = 0. \end{aligned} \tag{25}$$

They correspond to equations (26) and (27) of Mehl (2007), after correcting the sign of the second term of S_{ln0}, as pointed out by Mehl (2010).

2.4 MATLAB package

We have written a MATLAB package to compute acoustic modes in a gas-filled rotating spheroid, using perturbation theory. It is available under open-source license at `https://www.isterre.fr/annuaire/member-web-pages/henri-claude-nataf/`.

In order to save time for researchers who would like to apply Mehl's beautiful results, we list below our corrections to the main typos we found in the published version of Mehl (2007).

equation number	published version	corrected version
19	$j_l\left[(\xi_{ln})\right]^2$	$\left[j_l\left(\xi_{ln}\right)\right]^2$
27	$-\frac{1}{2\xi_{ln}^2}+\frac{j_0(\xi_{ln})}{2\xi_{ln}j_0'\xi_{ln}}$	$-\frac{1}{2\xi_{ln}^2}-\frac{j_0(\xi_{ln})}{2\xi_{ln}j_0'(\xi_{ln})}$
35	...	multiply the second member by -1
41	$r=\frac{a}{\sqrt{1+(2\varepsilon+\varepsilon^2)\sin^2\theta}}$	$r=\frac{a}{\sqrt{1+(2\varepsilon+\varepsilon^2)\sin^2\theta}}$
44	$B_{0020}^{(n)}=\frac{2\sqrt{5}}{15}\xi_{0n}^2$	$B_{0020}^{(n)}=-\frac{2\sqrt{5}}{15}\xi_{0n}^2$
45	$S_{0n0}=\frac{1}{4\xi_{0n}^2}$	$S_{0n0}=-\frac{1}{4\xi_{0n}^2}$
47 for A_{ln0ln0}	...	multiply the last term before $O(\varepsilon^3)$ by ε^2
47 for $A_{ln\pm1ln\pm1}$	$\frac{4\left(\xi_{ln}^2-3\right)}{5\left(\xi_{ln}^2-2\right)}\varepsilon$	$\frac{4\left(2\xi_{ln}^2-3\right)}{5\left(\xi_{ln}^2-2\right)}\varepsilon$
51 (denominator of ε^2 term)	$7875\left(\xi_{ln}^2-2\right)^2$	$7875\left(\xi_{ln}^2-2\right)^3$
53	$r=\frac{a}{\sqrt{1+(2\varepsilon+\varepsilon^2)\cos^2\theta}}$	$r=\frac{a}{\sqrt{1+(2\varepsilon+\varepsilon^2)\cos^2\theta}}$
55	$\langle\mathcal{F}_1\rangle=-\frac{2}{5}$	$\langle\mathcal{F}_1\rangle=-\frac{2}{15}$
57 (denominator of ε^2 term)	$7875\left(\xi_{ln}^2-2\right)^2$	$7875\left(\xi_{ln}^2-2\right)^3$
78	$-\frac{1}{2\xi_{ln}^2}+\frac{j_0(\xi_{ln})}{2\xi_{ln}j_0'(\xi_{ln})}$	$-\frac{1}{2\xi_{ln}^2}-\frac{j_0(\xi_{ln})}{2\xi_{ln}j_0'(\xi_{ln})}$ (as noted in Mehl (2010))

3 Elastic effects of the container

The finite elasticity of the ZoRo container allows a coupling between acoustic and elastic modes, modifying their eigenfrequencies (Moldover et al., 1986). Elastic eigenfrequencies of the ZoRo spheroidal shell container have been estimated with finite-element (COMSOL Multiphysics) and analytical calculations. In the latter case, the elastic influence on acoustic eigenfrequencies can be calculated with the thin-shell approximation (Rand and DiMaggio, 1967). This allows us to consider spherical and spheroidal containers. In the spherical geometry, this calculation can also be done without the thin-shell approximation by following Mehl (1985) or Lonzaga et al. (2011), who corrected some typos and gave also the modification of elastic modes due to the fluid coupling. The two approaches give very similar results and predict frequency shifts δ_{shell} from 0.1 to 1 Hz far from the eigenfrequencies, but δ_{shell} can reach 10 Hz near acoustic resonances. We have successfully compared those predictions with finite element calculations.

Further comparison with the experiment is difficult, due to the complex shell geometry (sensors holes, shafts, equatorial bulge, etc.) and the influence of the frame supporting the spheroid. Nevertheless, finite-element calculations confirm that these complexities do not modify the order of magnitude of elastic effects. Near acoustic resonances, elastic resonances can thus be one of the cause to the shifts left in the experimental spectrum that are unexplained by the finite-element computations. It can be noted that the sign of acoustic frequency shifts due to the shell elasticity is not uniform (it can either lower or raise acoustic frequencies). Yet, since the shifts are very small compared to the flattening effect, no mode switching should occur.

Coupling between the elastic shell and the outer surrounding fluid is expected to also possibly have an influence on the complex eigenfrequency, i.e. both on the frequency and on the damping rate of modes. Theoretical calculations on the modes $l = 0$ can be performed (Moldover et al., 1986), confirming finite-element predictions. This suggests that this effect is very small in ZoRo. Sound radiation in the surrounding air can thus be discarded in the interpretation of the ZoRo experimental results.

4 Numerical values for ZoRo's acoustic modes

For a selection of modes labelled by the radial mode number n and the angular mode number l, we give below: the mode frequency f_{nl}, the Ledoux coefficient C_{nl}, the ellipticity coefficient γ_{nl}, and the imaginary part of mode frequency due to dissipation g_{nl}.

n	l	f (Hz)	C_{nl}	γ_{nl}	g_{nl} (Hz)
0	0	0.00	NaN	0.0000	NaN
0	1	578.41	0.8573	−0.9144	0.2340
0	2	928.67	0.3869	−0.1505	0.3731
0	3	1254.34	0.2387	−0.0604	0.5135
0	4	1569.06	0.1683	−0.0325	0.6568
0	5	1877.42	0.1278	−0.0204	0.8030
0	6	2181.59	0.1018	−0.0140	0.9519
0	7	2482.73	0.0839	−0.0102	1.1035
0	8	2781.59	0.0709	−0.0078	1.2574
0	9	3078.65	0.0611	−0.0061	1.4136
0	10	3374.25	0.0534	−0.0049	1.5720
0	11	3668.63	0.0473	−0.0041	1.7323
0	12	3961.98	0.0423	−0.0034	1.8946
1	0	1248.59	0.0991	0.0000	0.0956
1	1	1650.66	0.0601	−0.4360	0.1311
1	2	2025.66	0.0424	−0.1013	0.1714
1	3	2385.18	0.0324	−0.0466	0.2145
1	4	2734.38	0.0260	−0.0270	0.2596
1	5	3076.09	0.0216	−0.0176	0.3063
1	6	3412.07	0.0184	−0.0125	0.3543
1	7	3743.49	0.0159	−0.0093	0.4035
1	8	4071.16	0.0140	−0.0072	0.4538
2	0	2146.63	0.0335	0.0000	0.1283
2	1	2558.04	0.0242	−0.4145	0.1519
2	2	2949.29	0.0188	−0.0979	0.1795
2	3	3326.88	0.0152	−0.0455	0.2094
2	4	3694.45	0.0128	−0.0265	0.2411
2	5	4054.30	0.0109	−0.0174	0.2742
3	0	3029.94	0.0168	0.0000	0.1568
3	1	3446.84	0.0132	−0.4079	0.1761
3	2	3847.44	0.0108	−0.0968	0.1984
3	3	4236.01	0.0091	−0.0450	0.2229

Table 1: For an air-filled sphere reference model with a sound speed $c = 343.2638$ m/s and a radius $a = 0.1966$ m.

5 Finite-element calculations with COMSOL Multiphysics

5.1 Built-in COMSOL (version 5.4) capabilities and limitations

Finite-element calculations, on which relies the commercial software COMSOL Multiphysics, allow calculating acoustic modes in arbitrary geometries, in particular in the exact geometry of ZoRo. In this section, we show how one can determine accurately the effects, on modes, of rotation and thermo-viscous diffusion with COMSOL. Indeed, these effects cannot be simply calculated using the acoustic (scalar) equation governing the pressure p, and require thus to consider the more complex (vectorial) Navier-Stokes equations governing the velocity field $\boldsymbol{u}$. This can be done using the aeroacoustics interface of COMSOL, but three-dimensional (3D) calculations are too costly to resolve the thin acoustic boundary layers, and the built-in axisymmetric interface discard any possible azimuthal dependency of the fields.

In order to perform efficient axisymmetric calculations with a 2D mesh and a possible azimuthal dependency, we have thus exploited the axisymmetry of our spheroidal geometry by assuming a periodic dependency $\exp[\mathrm{i}(\omega t + m\varphi)]$, with the imaginary unit i, the cylindrical coordinates (r, φ, z), the azimuthal wavenumber m, the time t and the angular eigenfrequency ω. Built-in COMSOL interfaces allow such 2D calculations for the acoustic equation but not for the Navier-Stokes equations, for which the built-in interface is limited to $m = 0$.

The scripts taking into account the following modified equations are available at https://www.isterre.fr/annuaire/member-web-pages/david-cebron/.

5.2 How to calculate COMSOL axisymmetric aero-acoustic modes with $m \neq 0$?

To consider a possible azimuthal flow v using the built-in COMSOL axisymmetric interface for aeroacoustics, we need an additional equation governing v, and the ansatz $\exp[\mathrm{i}(\omega t + m\varphi)]$ will add supplementary terms in every equation. Note also that additional terms are also required to take into account the rotation of the frame.

In practice, we have used two sets of axisymmetric COMSOL aero-acoustics interfaces in the frequency domain, such that equations (1)-(3) are solved for two sets of unknowns named $(\boldsymbol{u}, T, p)$ and $(\boldsymbol{u_2}, T_2, p_2)$, where $\boldsymbol{u} = (u, w)$ is the built-in unknown velocity field in the cylindrical coordinates, with the cylindrico-radial velocity component u, and the axial velocity w along the z axis. Note that the interface 'Heat transfer in Fluids' is not well suited since eigensolvers are not built-in COMSOL for this interface, while using the PDE interface is difficult since the axisymmetric interface is not built-in (r and z are surprisingly treated as Cartesian coordinates in the built-in PDE interface). Then, noting with a subscript 2 the quantities associated with the set of equations governing $(\boldsymbol{u_2}, T_2, p_2)$, the required additional equation is given by the equation governing the unknown T_2, which is formally the same as equation (3). Indeed, the (scalar) equation governing v is the same as the one governing T_2 provided that (i) the velocity $\boldsymbol{u_2}$ is replaced by $\boldsymbol{u}$, (ii) the density ρ_2 is replaced by ρ, (iii) we set $\lambda_2 = \mu_2 = 0$, such that the velocity $\boldsymbol{u_2}$ does not contribute to the eigenmode damping calculation, and $\lambda_2 = \mu$, $\alpha_2 = 0$, $C_{p_2} = 1$, $T_{02} = v_0$, with the basic state $\boldsymbol{u_0} = (u_0, w_0)$. Then, in the frame rotating at $\boldsymbol{\Omega} = \Omega\hat{\boldsymbol{z}} = 2\pi f_\Omega \hat{\boldsymbol{z}}$, the following source terms (due to $m \neq 0$ and rotation) have been calculated using the commercial software MAPLE (symbolic computations) and added in the COMSOL built-in equations. In cylindrical coordinates (r, φ, z), these source terms read

$$M = -\frac{\mathrm{i}\rho_0 m v}{r} - \frac{\mathrm{i}\rho m v_0}{r}, \tag{26}$$

$$F_r = -\rho_0\left[\frac{v_0}{r}(\mathrm{i}mu - 2v) - 2\Omega v\right] + \rho\left[\frac{v_0^2}{r} + 2\Omega v_0 + \Omega^2 r\right] - \frac{\mu}{r^2}\left(2\mathrm{i}mv + m^2 u\right) + \mathrm{i}m\left(\mu_B + \frac{\mu}{3}\right)\left(\frac{\partial_r v}{r} - \frac{v}{r^2}\right), \tag{27}$$

$$F_z = -\frac{\mathrm{i}\rho_0 m v_0 w}{r} - \mu\frac{m^2}{r^2}w + \left(\mu_B + \frac{\mu}{3}\right)\frac{\mathrm{i}m\partial_z v}{r}, \tag{28}$$

and

$$Q = -C_p \frac{\mathrm{i}}{r} \rho_0 m v_0 T + \alpha \frac{\mathrm{i}}{r} T_0 m v_0 p - \lambda \frac{m^2}{r^2} T, \tag{29}$$

$$Q_2 = -\rho_0 \left[\frac{v_0(\mathrm{i}mv + u) + u_0 v}{r} + 2\Omega u \right] - \rho \left[\frac{u_0 v_0}{r} + 2\Omega u_0 \right] - \frac{\mathrm{i}m}{r} p + \frac{\mu}{r^2} \left[2\mathrm{i}mu - (1+m^2)v \right] + \left(\mu_B + \frac{\mu}{3} \right) \left[\frac{\mathrm{i}m(\partial_r u + \partial_z w)}{r} + \frac{\mathrm{i}mu - m^2 v}{r^2} \right], \tag{30}$$

where the azimuthal velocity v is actually governed by the built-in temperature equation of COMSOL for T_2, and where Q_2 is the source term to add in the set of equations governing $(\boldsymbol{u_2}, T_2, p_2)$. Note that these supplementary terms have been simply obtained by subtracting, from the full equations, the equations in the particular case $v = m = \Omega = 0$ corresponding to the COMSOL built-in equations.

In all our calculations, we have actually considered a homogeneous basic state (we have checked that the centrifugal forces are negligible in the context of the ZoRo experiment) at 20°C, using the parameters of table 2. Note also that global rotation, via the Coriolis force, adds a supplementary family of eigenmodes named inertial modes (Greenspan, 1968). However, since the global rotation rate for ZoRo is small compared to the sound speed, there is no hybridization between acoustic and inertial modes (Vidal et al., 2020).

Table 2: Parameter values used in the COMSOL calculations, for homogeneous ambient pressure $p_0 = 1$ atm and temperature $T_0 = 20°$ (see p. 315 of Blackstock, 2001, for the chosen value of μ_B).

ρ_0	μ	μ_B	C_p	α	λ	β_T	γ	c
kg.m^{-3}	Pa.s	Pa.s	J.kg^{-1}.K^{-1}	K^{-1}	W.K^{-1}.m^{-1}	Pa^{-1}		m.s^{-1}
1.204	$1.81 \cdot 10^{-5}$	0.6 μ	1005.42	$3.41 \cdot 10^{-3}$	$2.58 \cdot 10^{-2}$	$9.87 \cdot 10^{-6}$	1.4	343.194

5.3 Boundary conditions and details on the numerics

To be as close as possible to the experiment, we impose at the fluid boundary a no-slip condition, i.e. $(u, v, w) = (0, 0, 0)$ in the frame attached to the rigid container, and a constant temperature. These conditions leads to a modification of the (complex) eigenvalue due to respectively the viscous and thermal boundary layers. Because of the large thermal conductivity of the metallic container of ZoRo compared to the one of air, the COMSOL calculations neglect the finite thermal conductivity of the container (which would modify the boundary heat loss and thus the thermal damping of acoustic modes). In the main calculations shown in the article, the finite elasticity of the boundary is also neglected (the boundary is assumed to be perfectly rigid, preventing any radiation of sound in the surrounding fluid). However, calculations with an elastic boundary (with and without a sound radiation in a surrounding fluid) have also been performed in order to validate the elasto-acoustic estimates of the theoretical perturbative calculation (see section 5.4 for details on these calculations).

In addition to eigenvalue calculations, COMSOL also allows us to calculate, in the frequency domain, the fluid response for a given excitation source. At the locations of the experiment audio speakers and taking into account the finite size of the audio speaker, we have thus prescribed a velocity $\mathrm{i}\omega$ at the boundary, both in the normal and tangential directions. Then, the pressure is recorded, in the COMSOL calculation, at the point where the electrets are positioned in the experiment (the finite size of electrets is neglected in COMSOL calculations). Finally, the fluid response is calculated for a large number of m, and the complete response is then simply obtained by summing the results obtained for each m.

In order to give an idea of the CPU time required for such calculations, one can consider the numerical calculations we have done to reproduce the acoustic spectrum measured experimentally between 500 Hz and 2335 Hz. For this calculation, the fluid response has been calculated for each m between 0 and 6 for $\sim$ 3000 well-chosen frequencies, with a step of 0.2 Hz near the resonance peaks and with typically 15 calculated frequencies between the acoustics peaks. To capture correctly the

thin boundary layers, we have used a fine mesh model with $\sim 160\,000$ degrees of freedom. Even if the calculation of a unique fluid response takes only $\sim$ 12s on a 6 cores desktop computer, we had to do $\sim 20\,000$ calculations, leading to a CPU time of 3 days on this computer. Thus, the calculation of the complete spectrum between 500 Hz and 3000 Hz (typical resolution of 0.2 Hz near the resonances), which requires to consider all the values of m between 0 and 8, has taken a full week of calculation (or 1 day using a 64 cores cluster).

Note finally that careful tests of numerical convergence have been systematically performed. We have checked that the boundary layers are well resolved, with several mesh points within the boundary layer thickness $\sqrt{\nu/f_t} = 100\,\mu$m, with $f_t = 2$ kHz the typical acoustic frequency and $\nu = \mu/\rho_0 = 2{\cdot}10^{-5}\,\mathrm{m}^2.\mathrm{s}^{-1}$ the typical air kinematic viscosity in experiments (the thermal boundary layer thickness is similar since the air Prandtl number is $Pr = \rho C_p \nu/\lambda = 0.7$). Our tests of numerical convergence (see appendix C of Vidal et al., 2020) show that, for a given number of degrees of freedom, increasing the elements order decreases (respectively increases) the accuracy of the calculated eigenfrequency (respectively damping). We have thus used systematically Lagrange elements of order 3 for the pressure and order 4 for the velocity and temperature.

5.4 Elastic container, boundary coupling and sound radiation in the surrounding outer fluid

COMSOL also allows built-in calculations of pure elastic modes of the container. Even without any shell model approximation, such calculations are not costly, which allows 3D calculations. Considering a linear elastic container with completely free boundaries, such 3D calculations give a (degenerate) fundamental mode at 2853 Hz for a 1 cm thick sphere of internal radius 0.2 m, with a Young modulus of 71 GPa, a Poisson's ratio of 0.33 and a density of $2810\,\mathrm{kg.m}^{-3}$. Considering now the 1 cm thick spheroidal geometry of ZoRo, of internal semi-axes 0.2 m and 0.19 m, this mode is split into a mode at 2807 Hz and another (degenerate) mode at 2854 Hz.

Now, if we consider the COMSOL built-in axisymmetric calculations of elastic modes with arbitrary m and the previously developed axisymmetric model for acoustic modes, one can modify the boundary condition to take into account the two-way coupling between elastic and acoustic modes. However, built-in axisymmetric models do not allow any axial boundary displacement on the symmetry axis. While this is not a problem for acoustic modes with a rigid boundary, this axial displacement constraint only allows us to recover the 3D elastic modes verifying this condition, but also leads to additional elastic modes (e.g. $m = 1$ additional modes). Having this issue in mind, we have performed axisymmetric calculations of elasto-acoustic (diffusive) modes to obtain insights and order of magnitude estimates, but we have also done 3D calculations of the diffusionless counterparts of these modes by considering the cheaper scalar acoustic equation (which neglects diffusion and rotation). For instance, both approaches give that, for a 1 cm thick sphere of internal radius 0.2 m, the elastic coupling leads to a 0.1% increase of the fundamental acoustic frequency (around 568 Hz), while the next acoustic eigenfrequency (around 912 Hz) is decreased by 0.01%. Calculations in the spheroidal geometry of ZoRo give similar results.

Finally, one can also add a surrounding fluid in order to allow sound radiation in the outer fluid. To do so, we have solved the scalar acoustic equation in the outer fluid, coupled to the outer boundary of the elastic container. In order to mimic a sound radiation in an infinite domain, we have to prevent any sound reflection at the outer (computational) boundary of the outer fluid domain. To do so, we have used the built-in perfectly matched layer (PML) of COMSOL, which is an additional surrounding domain where the acoustic waves are absorbed. Using the advised structured mesh for the PML region, we have thus performed elasto-acoustic calculations with sound radiation. These calculations have confirmed that the sound radiation can be largely neglected in the discussion of the experimental results of ZoRo.

6 Mode identification on experimental spectrum (complement to Fig. 2 of the main text)

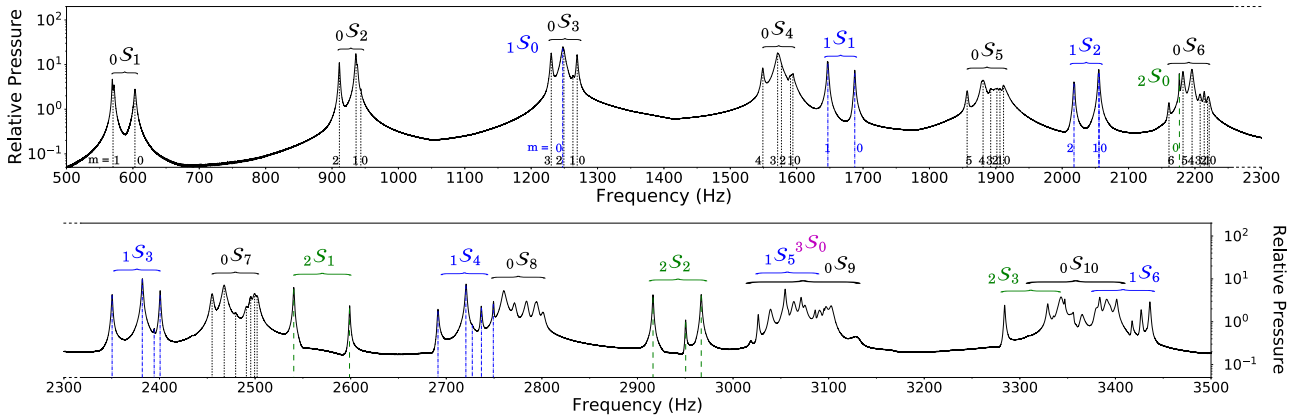

Figure 1: Experimental acoustic spectrum at rest, averaged over all electrets of one hemisphere. The spectrum is continued from top to bottom frame. Acoustic resonances are excited by speakers with a continuous linear chirp from 400 to 5000 Hz. Groups of peaks can be labelled with ${}_n\mathcal{S}_l$ according to theoretical prediction of a sphere of same volume (labels on brackets). Using the symmetry technique developed in III B, peaks can be systematically identified by their m numbers (dashed lines) up to 2500 Hz. Above this threshold, we can only identify some modes among those that are not too close.

7 Comparison of acoustic spectra from experiment, theory and finite-element calculations (complement to Fig. 6 of the main text)

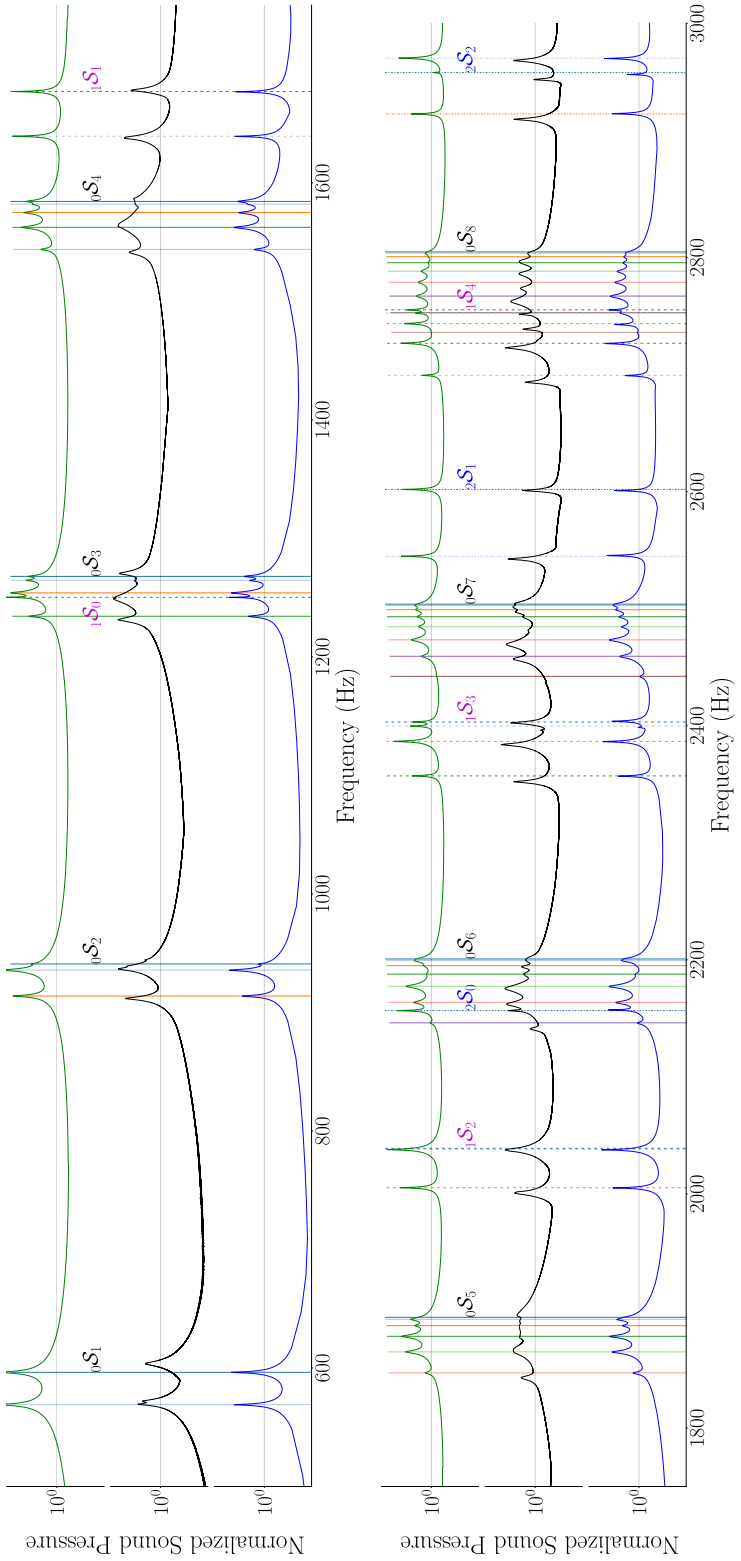

Figure 2: Acoustic spectra for ZoRo configuration at rest obtained with perturbation theory (top), experimental data (middle) and finite-element calculations (bottom). Mode frequencies and labels from the theory are given for comparison across the three spectra (vertical lines, different line types are used for n, different colours for m).

8 Examples of spectral fitting (complement to Fig. 8 of the main text)

We give here two examples of the fits of acoustic spectra performed for obtaining rotational splittings with the method described in the main text, and used to construct Fig. 8 of the main text.

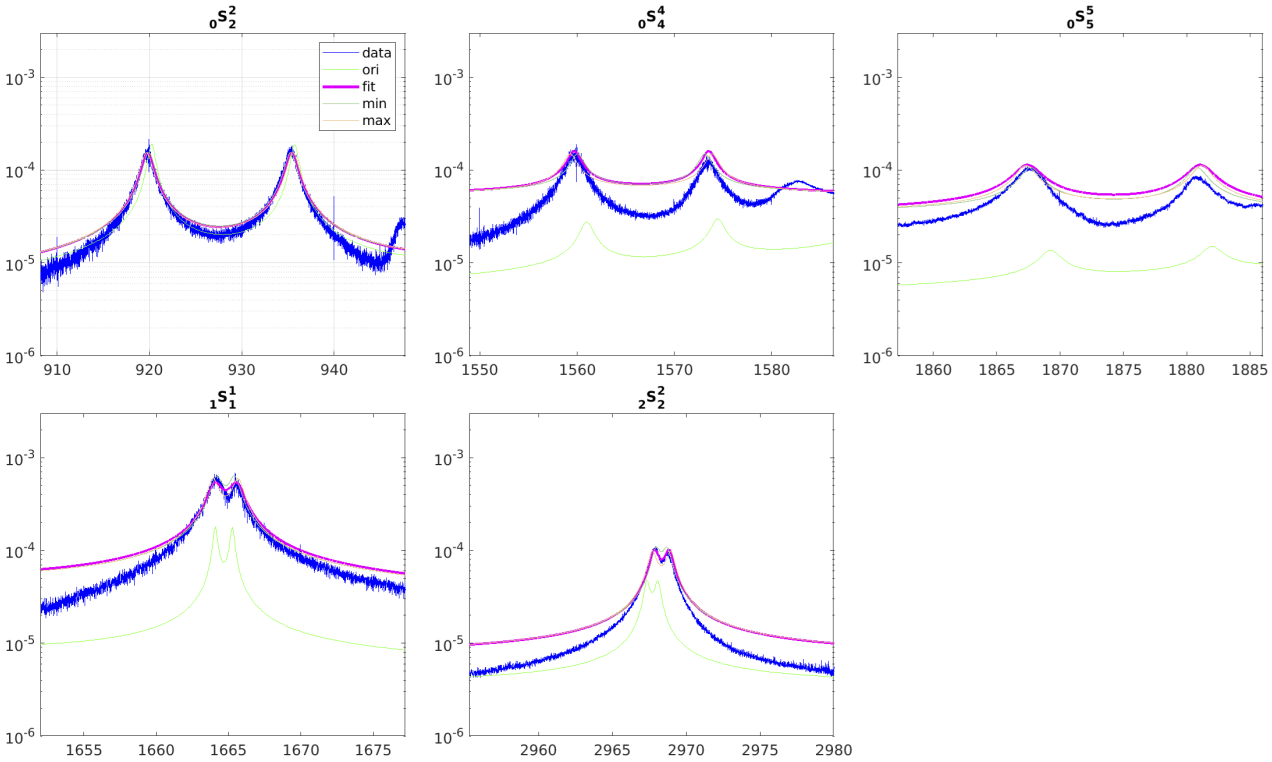

Figure 3: Experimental spectra (blue) for a selection of equatorially-symmetric acoustic modes for $f_\Omega = 10$ Hz, and synthetic spectra built with the method described in the main text. The thick magenta line is the best fit provided by the grid search, yielding the rotational splitting. The thin 'min' and 'max' lines are the spectra yielding the min and max acceptable splitting. The 'ori' green spectra is built with the 'nominal' parameters, used as a starting point of the grid search. Mode ${}_0\mathcal{S}_5^5$ is not considered as well fit and is thus discarded.

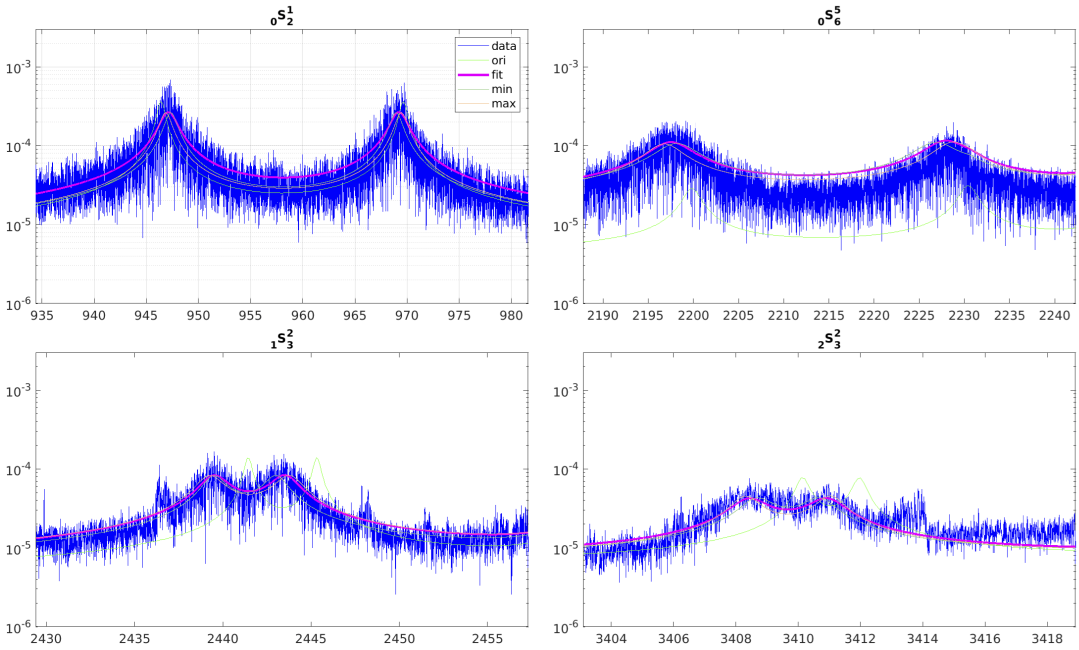

Figure 4: Same as Fig. 3 for a selection of equatorially-antisymmetric acoustic modes for $f_\Omega = 30$ Hz. Experimental spectra are much more noisy that at lower rotation rates, but can still be fitted. Mode ${}_2\mathcal{S}_3^2$ is not considered as well fit and is thus discarded.

9 Ledoux coefficients for a collection of symmetric and anti-symmetric modes (complement to Fig. 9 of the main text)

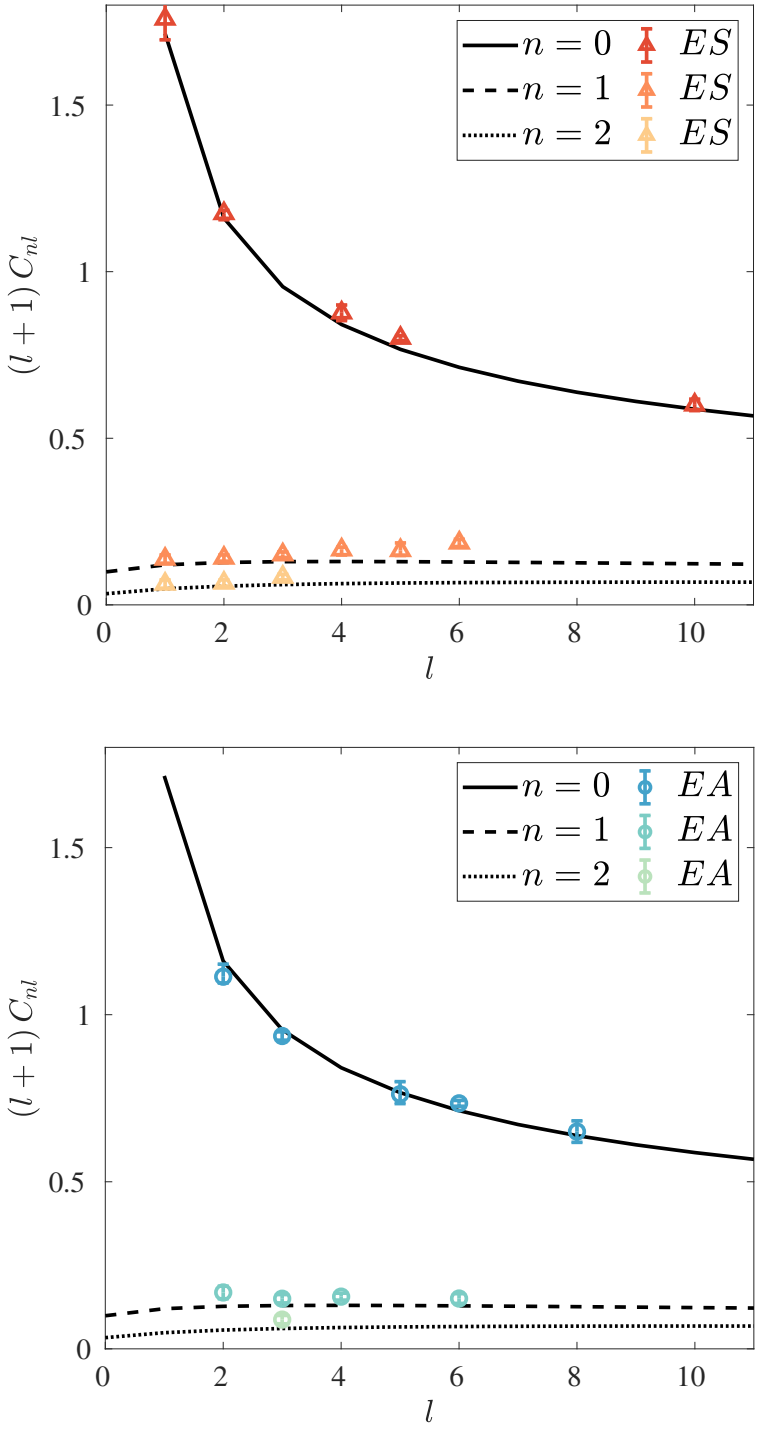

Figure 5: Comparison between the theoretical Ledoux coefficients (connected by lines for $n = 0$, 1, 2) and their experimental counterparts deduced from the mode splitting measured in ZoRo (spinning at 20 Hz) for several l-modes of various m. Top: symmetric modes with respect to the equator (ES, triangles), bottom: anti-symmetric modes with respect to the equator(EA, circles). When possible, several $\pm m$ pairs are included for one n, l pair. Note that we show $(l+1)\,C_{nl}$ on the vertical axis.

References

Blackstock, D. T. (2001). Fundamentals of Physical Acoustics.

Dahlen, F. (1976). Reply [to "Comments on 'The correction of great circular surface wave phase velocity measurements from the rotation and ellipticity of the Earth' by F.A. Dahlen"]. *J. Geophys. Res.*, 81(26):4951–4956.

Dahlen, F. and Tromp, J. (1998). *Theoretical Global Seismology*. Princeton University Press.

Dahlen, F. A. (1968). The normal modes of a rotating, elliptical Earth. *Geophys. J. Int.*, 16(4):329–367.

Greenspan, H. P. (1968). *The Theory of Rotating Fluids*. Cambridge University Press.

Lonzaga, J. B., Raymond, J. L., Mobley, J., and Gaitan, D. F. (2011). Suppression of an acoustic mode by an elastic mode of a liquid-filled spherical shell resonator. *J. Acoust. Soc. Am.*, 129(2):597–603.

Mehl, J. B. (1985). Spherical acoustic resonator: Effects of shell motion. *J. Acoust. Soc. Am.*, 78(2):782–788.

Mehl, J. B. (2007). Acoustic eigenvalues of a quasispherical resonator: second order shape perturbation theory for arbitrary modes. *J. Res. Natl Inst. Stan.*, 112(3):163.

Mehl, J. B. (2010). Acoustic eigenvalues of quasispherical resonators: beyond the triaxial ellipsoid approximation. *International Journal of Thermophysics*, 31(7):1259–1272.

Moldover, M. R., Mehl, J. B., and Greenspan, M. (1986). Gas-filled spherical resonators: Theory and experiment. *J. Acoust. Soc. Am.*, 79(2):253–272.

Morse, P. M. and Feshbach, H. (1953). *Methods of Theoretical Physics [Vol 1-2]*. McGraw-Hill, New York.

Rand, R. and DiMaggio, F. (1967). Vibrations of fluid-filled spherical and spheroidal shells. *J. Acoust. Soc. Am.*, 42(6):1278–1286.

Tritton, D. J. (2012). *Physical Fluid Dynamics*. Springer Science & Business Media.

Vidal, J., Su, S., and Cébron, D. (2020). Compressible fluid modes in rigid ellipsoids: towards modal acoustic velocimetry. *J. Fluid Mech. (in press)*.